Biomedical Signal Processing and Control 86 (2023) 105364

Contents lists available at ScienceDirect

Biomedical Signal Processing and Control

journal homepage: www.elsevier.com/locate/bspc

Enhanced brain efficiency network by integrating the new causality with fMRI and its application for Alzheimer's Disease study

Bocheng Wang , for the Alzheimer's Disease Neuroimaging Initiative[1]

College of Media Engineering, Communication University of Zhejiang, Hangzhou, Zhejiang 310018, China

ARTICLE INFO

Keywords:
Causality analysis
Efficiency network
Machine learning
HCP MMP
Alzheimer's Disease

ABSTRACT

The analysis of influence flow is crucial for the topological characterization of functional brain efficiency networks. Directional interaction among areal BOLD signals can be modeled by the causality method. Despite being widely used for studying Alzheimer's Disease in the brain, the Granger Causality (GC) has been shown to be unable to reveal true causality relationships through mathematical proof and simulation in EEG experiments. To evaluate its effectiveness in fMRI studies, first, we integrated a novel causality method called the New Causality (NC) with fMRI data. Both strong and weak causal impacts between stochastic processes were simulated and tested by GC and NC methods. Additionally, 1,893 patients in different stages of progression toward Alzheimer s disease were acquired and analyzed through the causality-based connectivity study. Finally, machine learning was employed to explore the performance in classification under these two methods. Simulation results show that compared to the GC, the NC method is more sensitive and reasonable to address causality relationships, especially for those weak causal impacts. Both the brain efficiency network and the classification performance can be enhanced through the NC introduction. Furthermore, it provides additional evidence supporting the critical involvement of the middle insular cortex, along with the temporal, parietal, and frontal lobes, in consciousness and functional diversion, with the help of NC integration.

1. Introduction

As the global population ages, millions of elderly individuals are experiencing varying degrees of decline in cognitive capabilities. Approximately 60–70 % of these cases deteriorate into Alzheimer's Disease (AD), which has significant physical, psychological, and social impacts on both patients and their families, as well as on society as a whole. Despite numerous hypotheses [1–3] proposed from the fields of neuroscience, genomics, and psychology for pathological research on AD, there is currently no effective way to intervene and treat the disease. For all that, it is highly possible to make early predictions for AD, as structural and functional alterations in the human brain have been widely found at the early stage of cognitive impairment onset. To conduct multimodal and longitudinal research for AD patients, thousands of subjects have been collected with clinical, imaging, genetic, and biochemical biomarkers data by the Alzheimer's Disease Neuroimaging Initiative (ADNI) decades ago. Different stages of mild cognitive impairment (MCI) have been grouped into the early MCI (EMCI), the late MCI (LMCI), the AD, and the health control (HC) according to their assessments in kinds of neuropsychological examinations [4].

Accurately predicting the early stages of AD is one of the greatest challenges in the world, and most studies have achieved superior recognition performance for binary classification. Rallabandi et al. [5] proposed an automated deep learning model based on the MRI and PET imaging modalities and achieved accuracies of 95.3 %, 94.1 %, and 96.2 % in classifying HC vs MCI, MCI vs AD, and AD vs HC respectively. Chai et al. [6] recruited 79 volunteers (40 MCI patients and 39 HC), extracted 68 features from the EEG signals, and designed an SVM model with a 96.3 % classification result. However, despite these efforts, multi-group classification for the refined groups of EMCI, LMCI, AD, and HC has not yet achieved the same level of performance as binary classification. Amoroso et al. [7] reported an accuracy of 38.8 % for the recognition of four classes with a random forest-based deep neural network. Sheng et al. [8] proposed a concept of ordered core features to reveal the functionality in the brain under two specifically progressive relationships, and an accuracy of 53.3 % was got in the four-group recognition

E-mail address: wangboc@cuz.edu.cn.

[1] Data used in preparation of this article were obtained from the Alzheimer's Disease Neuroimaging Initiative (ADNI) database (adni.loni.usc.edu). As such, the investigators within the ADNI contributed to the design and implementation of ADNI and/or provided data but did not participate in analysis or writing of this report. A complete listing of ADNI investigators can be found at: http://adni.loni.usc.edu/wp-content/uploads/how_to_apply/ADNI_Acknowledgement_List.pdf.

https://doi.org/10.1016/j.bspc.2023.105364
Received 4 May 2023; Received in revised form 15 July 2023; Accepted 14 August 2023
Available online 21 August 2023
1746-8094/© 2023 Elsevier Ltd. All rights reserved.

for HC, EMCI, LMCI, and AD against the baseline of 25 %. The low level of multi-group classification poses challenges for clinical diagnosis and early prediction of AD, and is typically hindered by two factors. First, the small number of available AD samples for machine learning. Compared to other successful domains engaging in artificial intelligence possessing massive amounts of data, AD-related AI models cannot be fully trained with the limited dataset in which situation it is inevitable to cause overfitting. Second, inappropriate feature engineering makes the model performance worse and inaccurate AD-related descriptions have few effects on model fitting.

Extensive connectivity studies have been conducted on the brain to investigate Alzheimer's pathology. Research [9] shows that functional alterations occur decades earlier than morphological changes which often present in the late stages of cognitive impairment. Connectivity is defined as the functional interactions among different areas of the brain, which can be evaluated by the EEG [10,11], DTI [12], or fMRI signals. As a result, more research is integrating connectivity-driven features into deep learning and conducting topological analysis of the brain, rather than solely observing structural characteristics such as volume atrophy in specific subregions [13,14]. Yu et al. [15] computed the global and local efficiency, the clustering coefficient and the betweenness centrality as topological features, and trained a TSK fuzzy machine learning model for AD identification with the highest accuracy of 97.3 %.

Previously, we explored the correlation-based connectivity within the fMRI BOLD signals and generated the connectivity matrix for each brain area. A novel joint HCPMMP method [16] was proposed to register the non-HCP standard ADNI MRI/fMRI data into 360 HCPMMP areas. The refined parcellation helped to observe subtle changes among the multimodal brain regions and to quantitatively measure the connectivity relationships. Followed by the analysis of topological variability, a vector of 5,414 features was set up to train a supervised learning model [8]. A distinct banding area was found which significantly differs in the cognitive impairment groups. Lately [17], by comparison to various cortex parcellation methods, the HCPMMP was further confirmed its effectiveness in modeling the connectivity, and weightings for each areal connectivity feature were established to describe the AD and its prodromal stages. However, correlation-based connectivity cannot depict the influence flow between brain areas, and the missing impact direction brings difficulty in the instruction of model tuning and explanation of the underlying functionality mechanisms in respect of brain working.

For this reason, the causality method is referred [18] to analyze the influence direction among brain areas, and differs from the correlation-based connectivity matrix, the causality-based matrix is termed as the effective network or brain efficiency. In literatures [19–22], the Granger causality (GC) is widely employed to measure the degree of interplay between time series. It is a statistical hypothesis test for determining whether one variable s past values contribute to predicting another. GC originated from the field of economics and was first introduced by Clive Granger in 1969 [23]. Over the past decades, the method has been extended to many domains such as the study of meteorology [24], sociology [25], and especially neuroscience. Caroline et al. [26] studied the classification performance for AD and schizophrenia patients with constructing the matrix of connections by using Granger causality, Pearson's and Spearman's correlations, and achieved higher than 0.9 scores of area under the ROC curve (AUC). Although it is widely used, recent studies [27,28] have pointed out that GC is unable to demonstrate the true causality through mathematical proof and simulation with the EEG experiments. To enhance the causality-based connectivity matrix and reveal the areal influence flow alterations among different stages of progression toward Alzheimer s disease, we integrated a novel causality definition with the fMRI BOLD signals, simulated the strong or weak causal influence between time series, and applied this method into the feature engineering of AD-related machine learning.

2. Method

2.1. Enhanced brain efficiency network

An enhanced brain efficiency network is introduced in this study. Generally, the efficiency is defined as the directional interaction of regional biological signals in the brain, which can be analyzed by causality modeling methods for time series [29]. Considering the following auto-regressive models in Eq. (1) in which X_1 and X_2 are stochastic processes that only accumulate values from their own past with white Gaussian noise ε that uncorrelated over time. t is for time, W is the coefficient that can be solved by the Least Square Method, and m corresponds to the maximum lagging term which can be determined by AIC criterion. Variance can be computed for ε_1 or ε_2 after fitting the coefficients W, and labeled as Σ.

$$\begin{cases} X_1(t) = \sum_{n=1}^{n=m} W_{1,n} X_1(t-n) + \varepsilon_1 \\ X_2(t) = \sum_{n=1}^{n=m} W_{2,n} X_2(t-n) + \varepsilon_2 \end{cases} \tag{1}$$

The causality relationship can be mathematically built in a joint-regression model in Eq. (2), and the variance Γ for error term η can also be computed by solving the optimal weightings. η_1 and η_2 have zero means. In the definition of Granger Causality [30], the causal impact is measured by the ln ratio between Σ and Γ. If the value of Γ is equal to Σ, it means that the introduction of X_2 does not help improve the prediction accuracy of X1, and the time series are independent. On the other hand, if the value of Γ is smaller than Σ, it means the joint of X_2 has a positive effect on improving the fitting of time series X_1.

$$\begin{cases} X_1(t) = \sum_{n=1}^{n=m} W_{11,n} X_1(t-n) + \sum_{n=1}^{n=m} W_{12,n} X_2(t-n) + \eta_1 \\ X_2(t) = \sum_{n=1}^{n=m} W_{21,n} X_1(t-n) + \sum_{n=1}^{n=m} W_{22,n} X_2(t-n) + \eta_2 \end{cases} \tag{2}$$

However, the above variance can only be measured by the difference between the fitting and the ground-truth value. Hu et al. [27] pointed the GC definition has its inherent shortcomings and/or limitations to illustrate the real strength of causality. A proportion-based causality named New Causality (NC) [28] was proposed to enhance the causality analysis capability for stochastic processes. Eq. (3) is the multivariate formulation generalized from the binary time series in Eq. (2). The small n is the total number of variables. In Eq. (4), $NC_{X_i \to X_k}$ is defined as the NC value from stochastic process X_i to X_k, N is the total length of observations, m is the lagging term computed by AIC criterion. In this study, only two time series of the simulated BOLD signals and the in-vivo fMRI data were considered. Thus, Eq. (4) can be simplified as Eq. (5).

$$\begin{cases} X_{1,t} = \sum_{j=1}^{m} a_{11,j}X_{1,t-j} + \cdots + \sum_{j=1}^{m} a_{1i,j}X_{i,t-j} + \cdots \\ \qquad + \sum_{j=1}^{m} a_{1n,j}X_{n,t-j} + \eta_{1,t} \\ X_{2,t} = \sum_{j=1}^{m} a_{21,j}X_{1,t-j} + \cdots + \sum_{j=1}^{m} a_{2i,j}X_{i,t-j} + \cdots \\ \qquad + \sum_{j=1}^{m} a_{2n,j}X_{n,t-j} + \eta_{2,t} \\ \cdots \\ X_{(k-m+1),t} = \sum_{j=1}^{m} a_{(k-m+1,1),j}X_{1,t-j} + \cdots + \sum_{j=1}^{m} a_{(k-m+1,i),j}X_{i,t-j} + \cdots \\ \qquad + \sum_{j=1}^{m} a_{(k-m+1,n),j}X_{n,t-j} + \eta_{k-m+1,t} \\ \cdots \\ X_{k,t} = \sum_{j=1}^{m} a_{k1,j}X_{1,t-j} + \cdots + \sum_{j=1}^{m} a_{ki,j}X_{i,t-j} + \cdots + \sum_{j=1}^{m} a_{kn,j}X_{n,t-j} + \eta_{k,t} \\ \cdots \\ X_{n,t} = \sum_{j=1}^{m} a_{n1,j}X_{1,t-j} + \cdots + \sum_{j=1}^{m} a_{ni,j}X_{i,t-j} + \cdots + \sum_{j=1}^{m} a_{nn,j}X_{n,t-j} + \eta_{n,t} \end{cases} \tag{3}$$

$$NC_{X_i \to X_k} = \frac{\sum_{t=m}^{N} \left(\sum_{j=1}^{m} a_{ki,j}X_{i,t-j}\right)^2}{\sum_{h=1}^{n}\sum_{t=m}^{N} \left(\sum_{j=1}^{m} a_{kh,j}X_{h,t-j}\right)^2 + \sum_{t=m}^{N} \eta_{k,t}^2} \tag{4}$$

$$NC_{X_1 \to X_2} = \frac{\sum_{t=m}^{N} \left(\sum_{j=1}^{m} a_{21,j}X_{1,t-j}\right)^2}{\sum_{t=m}^{N} \left(\sum_{j=1}^{m} a_{21,j}X_{1,t-j}\right)^2 + \sum_{t=m}^{N} \left(\sum_{j=1}^{m} a_{22,j}X_{2,t-j}\right)^2 + \sum_{t=m}^{N} \eta_{2,t}^2} \tag{5}$$

Hu et al. demonstrated the effectiveness of the NC method and applied it in the domain of EEG analysis. But for the fMRI data, the time resolution is not as good as EEG technology and is always accompanied by a large amount of sampling noise. Despite this, the excellent spatial accuracy of fMRI makes it one of the most successful brain imaging techniques. It is promising to extend the NC method to fMRI data and further enhance the brain efficiency network definition.

2.2. Simulation

To examine the effectiveness of NC-based brain efficiency network in fMRI data, two causal-related stochastic processes were simulated in this study. First, both strong and weak causality relationships were modeled in Eq. (6)–(7). $X(t)$ was defined in an auto-regression model and only correlated to itself past value with a large coefficient 0.9 plus a noise term η_1. In Eq. (6), time series Y was modulated by a strong causal impact from X compared to the past value of Y itself. While in Eq. (7), causal effects from Y itself exceeded the X factor 10 times. **A** is the coefficient which ranges from 0.01 to 0.1. Implemented in Matlab VARM function, the total time step in X and Y was set to 10 s.

$$StrongCausality = \begin{cases} X(t) = 0.9X(t-1) + \eta_1 \\ Y(t) = AX(t-1) + (0.1A)Y(t-1) + \eta_2 \end{cases} \tag{6}$$

$$WeakCausality = \begin{cases} X(t) = 0.9X(t-1) + \eta_1 \\ Y(t) = (0.1A)X(t-1) + AY(t-1) + \eta_2 \end{cases} \tag{7}$$

To simulate the BOLD signal, a canonical Hemodynamic Response Function with TR = 100 ms implemented in SPM toolbox (https://www.fil.ion.ucl.ac.uk/spm/) was convolved with X and Y as Alard Roebroeck et al. [31] suggested. Subsequently, these simulated BOLD responses were further down sampled every TR to simulate signal acquisition by the scanner. After normalization, these signals were added with 20 % white Gaussian noise to represent measurement error and noise in the acquisition. The whole simulation process was repeated hundreds of times. Both NC and GC causality methods were evaluated for these simulated BOLD signals.

2.3. In-vivo fMRI analysis

2.3.1. Sample preparation

To extend the NC method to fMRI analysis, different cognitive impairment and AD patients were acquired from the ADNI database. Table 1 lists the demographic and clinical characteristics of the samples used in this study. 597 patients for EMCI, 441 patients for LMCI, 266 patients for AD, and 589 for health control were downloaded. The imaging protocols for the structural MRI were as follows: Matrix X = 256.0 pixels, Matrix Y = 256.0 pixels; Matrix Z = 170.0; Pixel Spacing X = 1.0 mm; Pixel Spacing Y = 1.0 mm; Pulse Sequence = GR; Slice Thickness = 1.2 mm; TE = 3.2 ms; TI = 0.0 ms; TR = 6.8 ms; Weighting = T1. For the resting-state fMRI data, Matrix X = 64.0 pixels; Matrix Y = 64.0 pixels; Pixel Spacing X = 3.3 mm; Pixel Spacing Y = 3.3 mm; Pulse Sequence = GR; Slices = 6720.0; Slice Thickness = 3.3 mm; TE = 30.0 ms; TR = 3000.0 ms.

2.3.2. Brain parcellation

The HCP MMP cortex parcellation method [32] was employed in this study. There are 180 multi-modal cortical areas defined in each hemisphere respectively. It is considered one of the most fine-grained cortex parcellation up to date, which is driven by four kinds of modalities including morphology, functionality, topology, and connectivity. Due to its strict requirements for MRI/fMRI protocols, the J-HCPMMP [16] and DBCP [33] methods (http://dbcp.cuz.edu.cn/) were used to achieve cortex parcellation for the ADNI which held with lower imaging resolution than HCP and without T2w data. Specifically, these non-HCP data were passed to FreeSurfer [34] (https://surfer.nmr.mgh.harvard.edu/) and fMRIprep [35] (https://fmriprep.org/en/stable/) pipelines for their structural and functional preprocessing including slice timing, motion correction, artifact detection, co-registration, normalization, segmentation, and smoothing and so on. Subsequently, the registered MRI and fMRI data would be handled by CIFTIFY pipeline [36] (https://edickie.github.io/ciftify/) to map the T1w structure space into CIFTI space and down-sampled the gray-ordinates vertices into 32 K. The 180 HCP MMP areas were delineated in these cortical 32,492 vertices per hemisphere in which parcellated BOLD signals could be extracted through HCP wb_command CIFTI-PARCELLATE [37] (https://www.humanconnectome.org).

2.3.3. Effective network evaluation

The effective network was evaluated using both NC and GC methods based on these parcellated BOLD signals. The time series from each

Table 1
Demographic and Clinical Characteristics.

	HC	EMCI	LMCI	AD
Total Number	589	597	441	266
Male/Female	282/307	338/259	225/216	149/117
Age	72.08 ± 11.91	70.26 ± 8.79	69.26 ± 13.17	73.52 ± 10.97
Education Years	16.13 ± 3.25	16.17 ± 2.94	16.54 ± 3.58	15.57 ± 3.00
CDR	0.04 ± 0.14	0.46 ± 0.19	0.56 ± 0.36	0.89 ± 0.41
MMSE	28.89 ± 1.88	28.09 ± 2.21	26.63 ± 3.43	21.59 ± 3.71
NPI	1.48 ± 4.63	4.10 ± 7.04	5.55 ± 8.93	7.88 ± 9.81
GDS	0.76 ± 1.24	1.89 ± 1.87	1.86 ± 2.04	1.72 ± 1.70
FAQ	0.27 ± 1.35	2.60 ± 4.22	5.31 ± 6.93	14.89 ± 7.69
ADAS	8.59 ± 4.95	12.27 ± 6.71	19.09 ± 10.79	33.01 ± 11.10

CDR: Cognitive Dementia Rating. MMSE: Mini-Mental State Examination. NPI: Neuropsychiatric Inventory. GDS: Geriatric Depression Scale. FAQ: Functional Activities Questionnaire. ADAS: Alzheimer's Disease Assessment Scale.

cortical area were first scaled to the range of (0,1). Then, two BOLD signals were iteratively chosen from mutually exclusive brain regions. One signal was designated as the independent variable X, while the other signal was designated as the dependent variable Y. Repeating this process resulted in 129,000 directional causality values, $n_{Area_i \to Area_k, where i,k \in (1,360)}$ for each of the 1,893 ADNI subjects, which produced a total 200 million causality values represented in size of 360 × 360 effective networks. Finally, Kruskal-Wallis, ANOVA, and Post Hoc tests were conducted to determine which directional causality values were significantly different among the four groups. These causality values were then used as input features for machine learning.

2.3.4. Machine learning

Several machine learning algorithms including the support machine learning (SVM), factorization machine (FM), K-nearest neighbors (KNN), and the unsupervised K-means method were tested to reduce model bias and to examine the discriminative capability of significant directional causality values located in paired cortex regions. The dataset was split into training, validation, and testing sets in a ratio of 0.6:0.2:0.2. To avoid overfitting, a four-fold cross-validation was used. The training and validation sets were divided into four equal subsamples. Then, a four-step iteration was carried out. In each step, a single subsample of the four subsamples retained as the validation data for testing the model, and the remaining three subsamples are used as training data. To ensure comprehensive evaluation of the model's performance, this four-step iteration was repeated four times, with each of the four subsamples used exactly once as the validation data. This approach allowed both the training and validation sets to be used four times, while the testing set was used only once to estimate the model's final performance. Classification performance was evaluated by a binary group confusion matrix. Accuracy, precision, sensitivity, and specificity were calculated using the Scikit-learn toolbox (https://scikit-learn.org/stable/).

3. Results

Fig. 1 displays the overall workflow of this study. The upper left row illustrates the generation of the simulated fMRI BOLD signal, while the bottom row shows the preprocessing procedure for the ADNI data. The right panel depicts the efficiency analysis performed using both the NC and GC methods for both the simulated and in-vivo fMRI data.

Fig. 2 shows the whole simulation process in which an autoregression time series X (A1-E1, in green) and the corresponding causally affected joint-regression time series Y (A2-E2, in purple) are generated. Lines in Fig. 2A are the original time series created by the Matlab VARM function. The autoregression coefficients and associated lags computed by the AUTOCORR method are drawn in red points in Fig. 2B. Obvious declining autocorrelation trend can be observed for series X, while only one significant autocorrelated point (Fig. 2B, Lag = 1) in Y can be obtained due to their mathematical definitions. Both X and Y are convolved with the canonical HRF function (Fig. 2C), down-sampled (Fig. 2D), and added with 20 % Gaussian noise (Fig. 2E).

Fig. 3 illustrates the causal impact from time series X to Y, represented for both strong (left) and weak (right) causal relationships. The simulation function of MATLAB was used to generate 200 random causal pairs (Test 1, Test 2, …, and Test 200), and both the NC and GC methods are examined. The GC test value is within the range of [0, +∞), for NC, the value locates in [0, 1], both are continuous numbers. These GC and NC values could be compared after the Min-Max normalization method. In the strong group (Fig. 3A), explicit causal impacts can be detected in both methods for most scenarios (Test 1, Test 50, and Test 100, areas filled in green, namely results match the simulation model), while for specific random simulations (e.g., Test 200), Granger causality turns to a contrary result that opposite causal impact from Y to X is exhibited (Wrong conclusions, areas filled in red. From the simulation models, X is an independent variable that only affected by itself past values). The performance of the GC method deteriorates as the lag increases. For the weak situation (Fig. 3B), an incorrect causal relationship under the GC method appears across the entire range of lag values (Test 1 and Test 200 in the early stage, Test 50 and Test 100 in the middle stage, Test 1, and Test 100 in the late stage). Furthermore, the NC method exhibits higher causal sensitivity compared to the GC method, as demonstrated by the larger area between the lines representing causality from X to Y and from Y to X.

In the in-vivo fMRI BOLD signal experiments, 1,893 directional causality matrices representing the efficiency in brain functional networks are calculated first. Each matrix is composed of 129,600 (360 × 360) causality values detected in fMRI BOLD signals between brain Area (i) and Area(j), where Area(i) and Area(j) locate in the regions of HCP MMP 360 cerebral cortex parcellation. Followed by a Kruskal-Wallis's test, nearly three-quarters of causality values are excluded due to their statistical insignificance during the difference detection among the four classes. Only 32,974 directional causal values in the NC method and 28,084 in GC exhibit significant differences in distinguishing cognitive impairment and AD patients. To further clarify the specific causal difference through multiple comparisons, a posthoc pairwise test with p-value adjusted (Benjamini/Hochberg method) is carried out. Those significant four-class sensitive causal values are counted and listed in Table 2. By counting the significant causal impacts between brain areas using both the NC and GC methods, a larger number of brain functional causal relationships could be seen in the HC and EMCI groups compared to those in the LMCI and AD groups. This suggests a significant

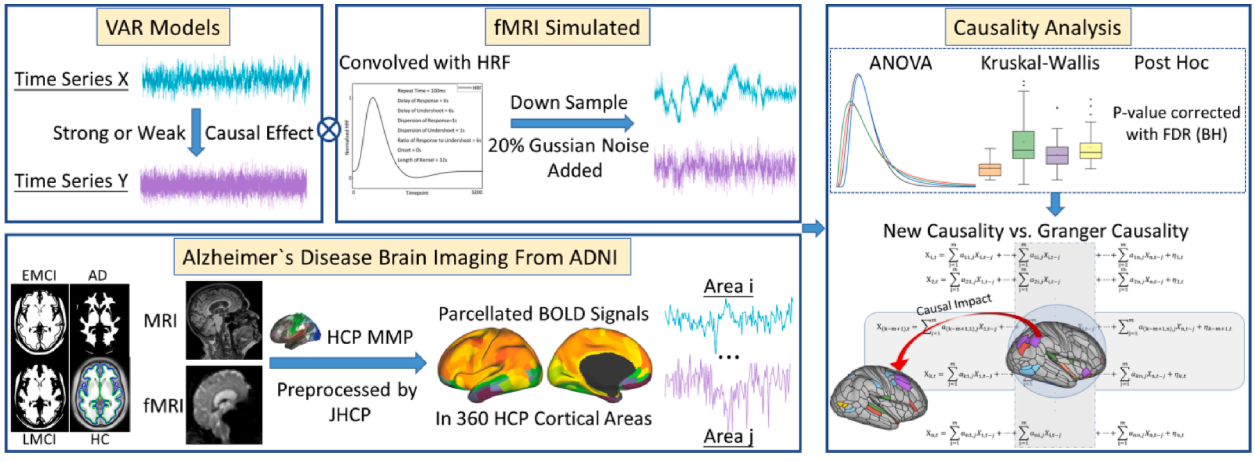

Fig. 1. Work flow in this study.

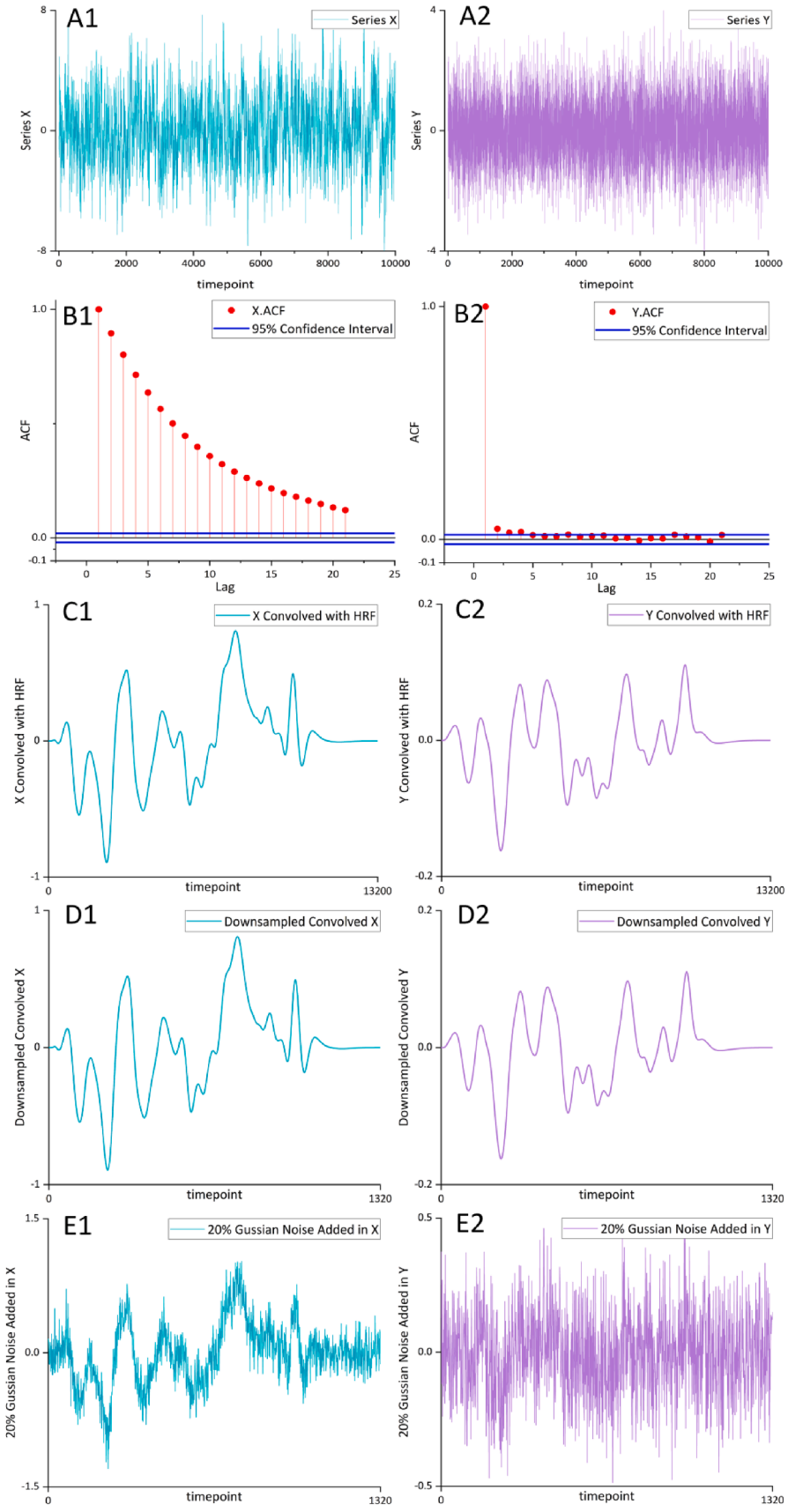

Fig. 2. Simulation of causal impacted fMRI BOLD signal. (A1-E1) the independent time series X, and (A2-E2) the causality impacted Y series.

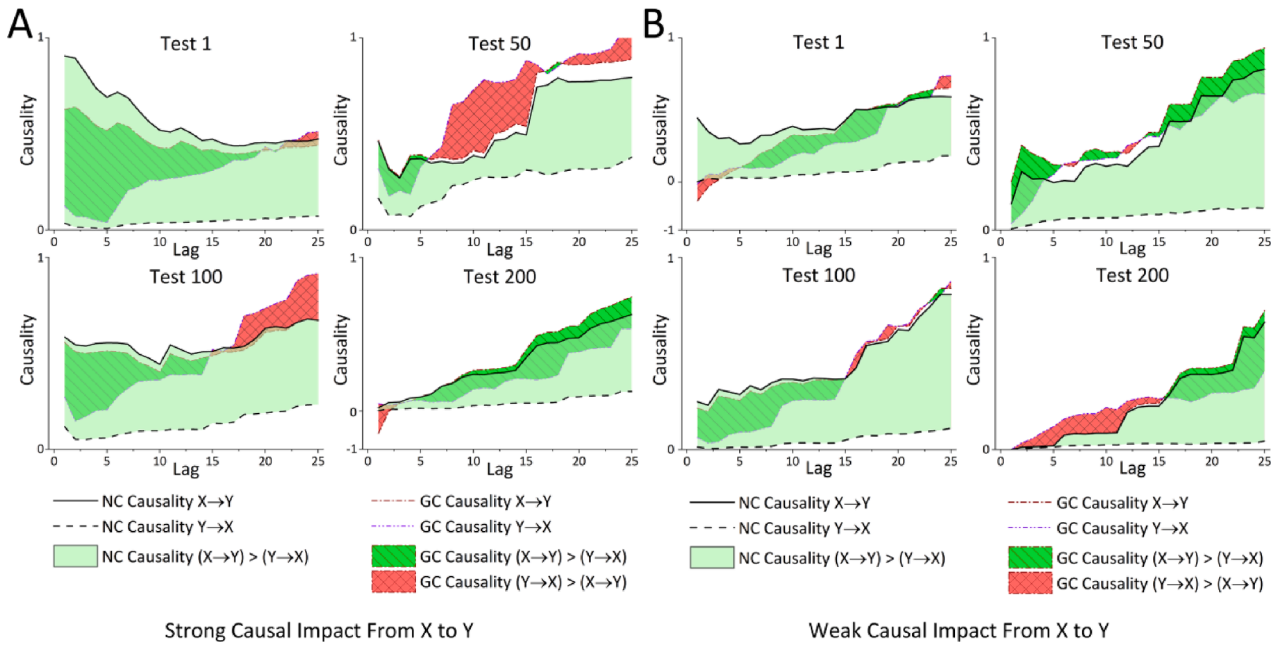

Fig. 3. Detection of strong (A) and weak (B) causal impact between two simulated fMRI BOLD signals.

Table 2
Counting of significant causal impact between areas after non-parametric statistics and post-hoc test.

	Difference Between	P-value	Total in NC	Total in GC
HC	HC vs. EMCI HC vs. LMCI HC vs. AD	'and' <0.05	839	762
EMCI	EMCI vs. HC EMCI vs. LMCI EMCI vs. AD	'and' <0.05	1346	944
LMCI	LMCI vs. HC LMCI vs. EMCI LMCI vs. AD	'and' <0.05	20	23
AD	AD vs. HC AD vs. EMCI AD vs. LMCI	'and' <0.05	100	138

difference in brain functionality among the EMCI, LMCI, AD, and HC groups. The strength of the causality relationship between different regions of the healthy brain is much stronger than that of a severely impaired cognitive brain.

Next, Fig. 4 illustrates the performance of machine learning models which are trained with those significant causality values derived from the NC method (in solid green) and the GC (in dotted orange). According to the results in Table 2, four groups of candidate features are initialized for the six pairwise classifications. Namely, the 839, 1346, 20, and 100 values are used as inputs for model training in (HC vs. EMCI), (HC vs. LMCI), (HC vs. AD), (EMCI vs. LMCI), (EMCI vs. AD), and (LMCI vs. AD) classification. For comparison, the 762, 944, 23, and 138 GC values are also trained in models. Thus, performances of HC, EMCI, AD, and LMCI features are shown in Fig. 4 (A–D). Among the forty-eight (4×6, for NC and GC) groups, causality features calculated by the NC method generally perform better in machine learning than those by GC. The highest acc scores in the pairwise classifications are drawn in Fig. 4E, from which it can be observed that the model trained with AD-related features achieves the best discrimination. Fig. 5 shows the confusion matrix with AD-related features calculated by NC and GC methods. The NC method exhibits better classification capability, as demonstrated by the larger number of true-positive (TP) and true-negative (TN) predictions located on the main diagonal.

To further analyze the topological characteristics of these causality influences in AD brains, the in-degree and out-degree statistics were carried out, and Fig. 6 shows the results. Principally, only AD-related features (100 values in NC, Table 2) those achieving the highest acc scores are presented here. Among the 100 directional causality influences, there are only two HCP MMP areas (L-MT and L-8Av) exhibit in-degree greater than or equal to 2. The rest causality links only occur once counting for in-degree. Regarding the out-degree, three areas L-7m, R-PCV, and R-MI have a causal influence on more than two other areas. Table 3 lists these causality relationships described in Fig. 6.

4. Discussion

Despite the superior spatial resolution of fMRI data, an indirect measure of neural firing brings lots of noise in BOLD signals which makes it difficult to achieve practical causality analysis [38]. Compared to GC, NC has been proven better in revealing the true causality in the EEG domain ascribing to its natural higher time resolution. To examine the performance of extending the NC definition to fMRI analysis, both strong and weak causality relationships were simulated by establishing the joint-regression models, and NC was further applied in the generation of brain effective network for cognitive impairment analysis in this study.

4.1. Enhanced brain efficiency network for weak causal impact in fMRI data

This is the first time that the NC method has been extended to the analysis of fMRI data. In general, the brain network can be measured by calculating correlation coefficients between BOLD signals. The directionless interaction is insufficient to explain the sophisticated causal flow among cortical functions. While the GC method is widely used in many domains, Hu et al. pointed out its theoretical and experimental flaws. This study provides further evidence that the NC method can reveal causal influences closer to the truth, particularly for weak impacts in fMRI data, as demonstrated by the simulation of both strong and weak causal relationships (Fig. 3B). The influence from X to Y is more distinct in NC causality, as evidenced by the significant gap between the upper solid curve (X → Y) and the bottom dotted curve (Y → X). Under GC causality, the gap is very narrow, and in some cases, the causality

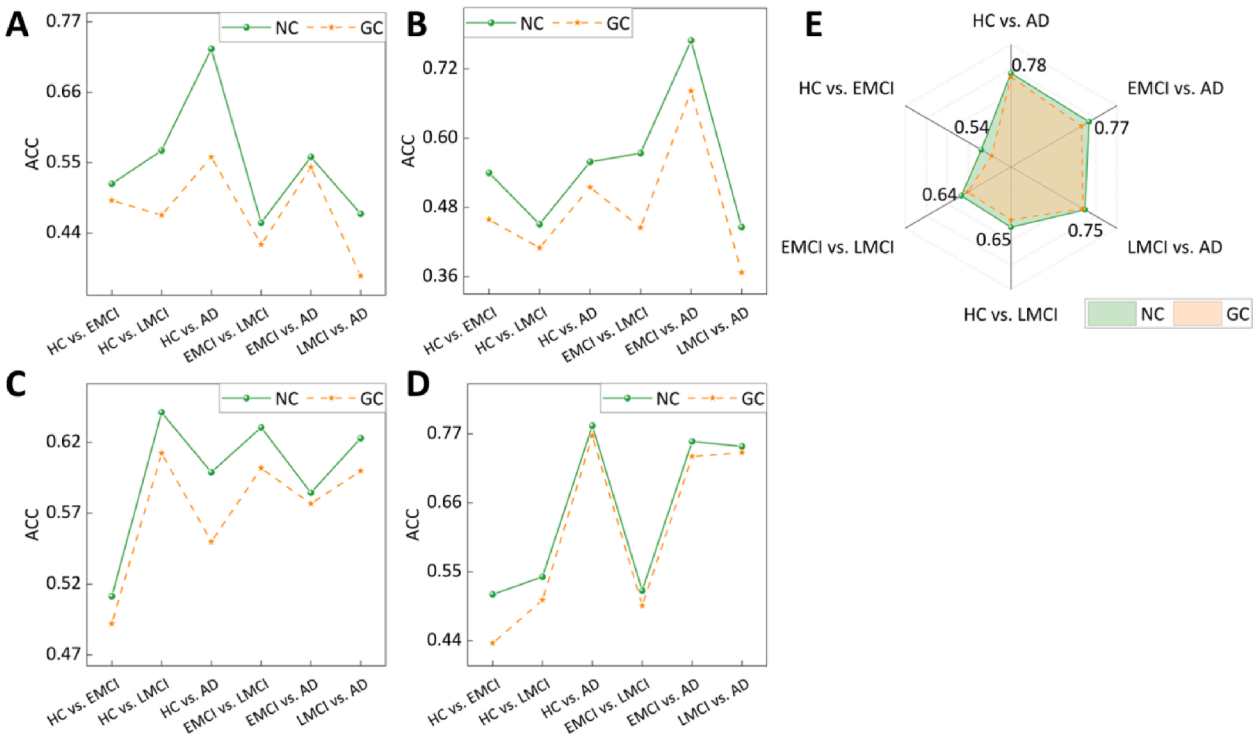

Fig. 4. Performance of forty-eight pairwise classifications with four-sensitive groups of causality features. Features of (A) HC-related, (B) EMCI-related, (C) AD-related, and (D) LMCI-related. (E) The highest acc achieved in each pairwise classification.

direction is completely inverted, as indicated by the red area. For the simulation of strong causal impact from X to Y (Fig. 3A), the vast majority of the causality influence can be accurately detected when the Lag is small. However, as the Lag increases, opposite causality conclusions may be drawn, suggesting that Y has a causal impact on X. The simulation results indicate that integrating the NC method enhances the evaluation of brain efficiency networks in fMRI compared to the GC method.

4.2. Enhanced directional causality analysis for cognitive impairment

For in vivo fMRI analysis, BOLD signals from different stages of cognitive impairment and AD patients were preprocessed using the HCP MMP method, which provides the most fine-grained cortical parcellation, and a size of 360 × 360 efficiency network was computed for each subject. Nearly three-quarters of the causality values in the network did not pass the significance test and were therefore excluded. Topological analysis was performed on the remaining directional causality relationships. In Fig. 6 and Table 3, the inferior parietal cortex (L-IP0 newly discovered, and L-IP2), the lateral temporal cortex (R-PHT), the temporo-parieto-occipital junction (R-TPOJ2 newly discovered), and the auditory association cortex (R-47L) exhibited a combined causal impact on L-8AV which locates in the dorsolateral prefrontal cortex (DLPFC) and was a newly discovered brain region in HCP MMP 2016. The posterior cingulate cortex (R-31a newly discovered), the primary somatosensory cortex (R-2), the dorsal stream visual cortex (R- IPS1), and the superior parietal cortex (R-AIP newly discovered) showed a combined causal impact on L-MT. Meanwhile, the posterior cingulate cortex (L-7m and R-PCV) and the middle insular area (R-MI) simultaneously causally impacted a great many cortical regions including the posterior cingulate cortex (L-31a newly discovered, L-23c, R-d23ab), the insular and frontal opercular cortex (L-52, R-FOP4 newly discovered), the anterior cingulate and medial prefrontal cortex (R-25), the early auditory cortex (L-RI, R-PBelt newly discovered), the dorsal stream visual cortex (R- IPS1), and the early visual cortex (R-V8). All these mentioned cortical areas have been broadly reported [39–41] as closely related to cognitive impairment in respect of wording memory, decision-making, and social cognition. Seven causality influence flows were found to pass through the middle insular area, regardless of whether it served as the in-degree or out-degree, highlighting its importance as a mandatory node in the efficiency network. It is consistent with previous studies [42,43] that the MI cortex plays a key role involved in consciousness and functionality diversion in conjunction with the temporal, parietal, and frontal lobes. The integration of HCP MMP and NC methods allows for the identification of more delineated causality relationships, as demonstrated by these findings, compared to those obtained using the coarse brain definitions in Brodmann areas or the directionless, correlation-based functional brain network.

4.3. Enhanced classification performance compared to GC in machine learning

Granger causality-based feature engineering is commonly used in machine learning for the prediction of brain pathology patients [26,44,45]. For comparison, in Fig. 4 and Fig. 5, the four-group sensitive features were used to train different kinds of machine learning models. Of the 48 pairwise classifications, all accuracy tests using NC features showed superior performance compared to those using GC features. While both GC and NC AD-related features scored close to 0.78 in the comparison of healthy controls (HCs) and AD patients, the calculation of HC-related causality using NC (0.75) was able to distinguish between patients and the same group of healthy controls by 20 percentage points more than GC (0.55). A similar scenario could be observed in the curves of the EMCI vs. LMCI group tested by EMCI-related features that the accuracy in NC was 15 percent higher than those of GC. These results demonstrate that subtle alterations in the groups of healthy controls vs. EMCI, EMCI vs. LMCI, and LMCI vs. AD can be accurately captured by the NC method during model training. This finding confirms the results of the simulations, which showed that weak causality relationships could be more accurately revealed using NC than GC. The improved classification performance in machine learning is attributed to the enhanced definition of brain efficiency networks.

AD Features by NC method

HC vs. EMCI		Prediction	
		HC	EMCI
TRUE	HC	76	90
	EMCI	105	75

HC vs. LMCI		Prediction	
		HC	LMCI
TRUE	HC	103	69
	LMCI	78	47

HC vs. AD		Prediction	
		HC	AD
TRUE	HC	152	21
	AD	34	47

EMCI vs. LMCI		Prediction	
		EMCI	LMCI
TRUE	EMCI	104	73
	LMCI	69	50

EMCI vs. AD		Prediction	
		EMCI	AD
TRUE	EMCI	145	29
	AD	32	46

LMCI vs. AD		Prediction	
		LMCI	AD
TRUE	LMCI	105	29
	AD	22	48

AD Features by GC method

HC vs. EMCI		Prediction	
		HC	EMCI
TRUE	HC	90	70
	EMCI	98	88

HC vs. LMCI		Prediction	
		HC	LMCI
TRUE	HC	112	57
	LMCI	79	49

HC vs. AD		Prediction	
		HC	AD
TRUE	HC	155	23
	AD	36	40

EMCI vs. LMCI		Prediction	
		EMCI	LMCI
TRUE	EMCI	106	62
	LMCI	87	41

EMCI vs. AD		Prediction	
		EMCI	AD
TRUE	EMCI	144	23
	AD	44	41

LMCI vs. AD		Prediction	
		LMCI	AD
TRUE	LMCI	94	19
	AD	34	57

Fig. 5. Confusion matrix with AD-related features.

4.4. Limitation

There are several aspects that could be improved in future research. First, the causality values that failed the significance test caused a large number of zeros in the brain efficiency network, resulting in extremely sparse matrices. This could pose a considerable hindrance in subsequent machine learning, particularly for the weighting solving in SVM or deep learning. Although sparse features in the 360 × 360 matrix were transcoded with a one-hot strategy and compressed under a factorization machine, we haven't achieved ideal binary classification accuracy as ideal as other studies [46] that prepare features with the directionless correlation matrix. The accuracy of 0.78 in AD classification may represent the true model performance due to our sufficient samples in training and testing while most studies [8,16,17] up-to-date only collect dozens or hundreds of AD-related samples in which accuracy exceeds 0.90 may have resulted from overfitting. Nevertheless, directional influence flow measured by the NC method is crucial for efficient network analysis, especially important for those weak causal-oriented BOLD signals glutted with inevitable noise among brain areas. Second, only in/out node degree was analyzed for each brain area in this study, while sophisticated topological analysis should be given that aspect of functionality communication or centrality alteration is of extreme importance to deeply understand the working mechanism of the brain.

5. Conclusion

To demonstrate the superiority of the introduced NC method in the brain efficiency network, the simulation of BOLD signals was used to model different degrees of causality relationships. Causal impacts especially the weak ones could be sensitively detected through the NC compared with the GC method. Performances of the directional causality analysis and classification for the cognitive impairment were both enhanced. Current clinical diagnoses for neurological diseases still heavily rely on subjective psychological scales (e.g., CDR, MMSE, GDS, etc.) and morphological changes that are often observable through neuroimaging only in the late stages of dysfunction. Simultaneously accompanied by fMRI acquisition, the proposed method integrated with functional connectivity evaluation can be employed as an essential supplementary means for the identification of brain disorders especially in their early stage. Further experiments are needed to study the statistical characteristics under the NC definition. Such experiments could lead to improvements in clinical diagnostic accuracy for patients with cognitive impairments.

CRediT authorship contribution statement

Bocheng Wang: Conceptualization, Methodology, Software, Visualization.

Declaration of Competing Interest

The authors declare that they have no known competing financial interests or personal relationships that could have appeared to influence the work reported in this paper.

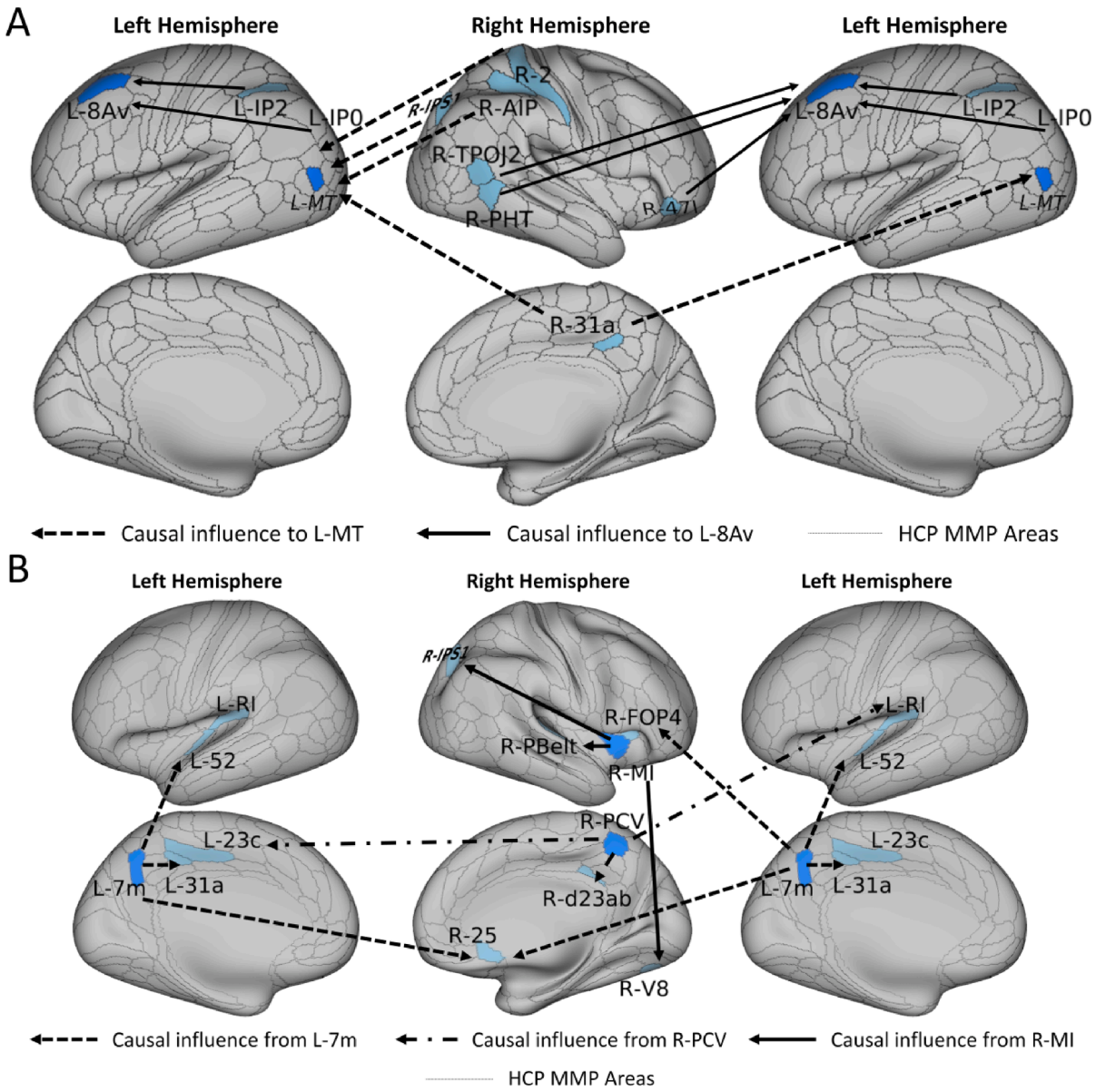

Fig. 6. Causality influence links which in/out degree larger than 2.

Table 3
Causality influence links used as the AD-related features.

Topological Characteristics	From	To
In-degree > 2	L-IP0	L-8AV
	L-IP2	
	R-PHT	
	R-TPOJ2	
	R-47L	
	R-31a	L-MT
	R-2	
	R-IPS1	
	R-AIP	
Out-degree > 2	L-7m	L-31a
		L-52
		R-25
		R-FOP4
	R-PCV	L-23c
		L-RI
		R-d23ab
	R-MI	R-IPS1
		R-PBelt
		R-V8

Data availability

All data are available on request. The preprocessing platform is available (http://dbcp.cuz.edu.cn), which allows great freedom in usage.

Acknowledgments

This work was supported by the High-level Scientific Innovation Cultivation Project for Young Doctors in the Communication University of Zhejiang (2023). Data collection and sharing for this project was funded by the Alzheimer's Disease Neuroimaging Initiative (ADNI) National Institutes of Health Grant U01 AG024904.

References

[1] N. Altomari, F. Bruno, V. Laganà, N. Smirne, R. Colao, S. Curcio, R. Di Lorenzo, F. Frangipane, R. Maletta, G. Puccio, A.C. Bruni, A comparison of behavioral and psychological symptoms of dementia (BPSD) and BPSD sub-syndromes in early-onset and Late-onset Alzheimer's disease, JAD 85 (2022) 691–699, https://doi.org/10.3233/JAD-215061.

[2] C.M. Lill, L. Bertram, Genome-wide analysis furthers decoding of Alzheimer disease genetics, Nat. Rev. Neurol. 18 (2022) 387–388, https://doi.org/10.1038/s41582-022-00678-x.

[3] K. Herrup, Fallacies in neuroscience: the Alzheimer's edition, ENeuro 9 (2022) ENEURO.0530-21.2021, doi: 10.1523/ENEURO.0530-21.2021.

[4] S.G. Mueller, M.W. Weiner, L.J. Thal, R.C. Petersen, C.R. Jack, W. Jagust, J. Q. Trojanowski, A.W. Toga, L. Beckett, Ways toward an early diagnosis in Alzheimer's disease: the Alzheimer's Disease Neuroimaging Initiative (ADNI), Alzheimer's & Dementia 1 (2005) 55–66, https://doi.org/10.1016/j.jalz.2005.06.003.

[5] V.P. Subramanyam Rallabandi, K. Seetharaman, Deep learning-based classification of healthy aging controls, mild cognitive impairment and Alzheimer's disease using fusion of MRI-PET imaging, Biomed. Signal Process. Control 80 (2023), 104312, https://doi.org/10.1016/j.bspc.2022.104312.

[6] J. Chai, R. Wu, A. Li, C. Xue, Y. Qiang, J. Zhao, Q. Zhao, Q. Yang, Classification of mild cognitive impairment based on handwriting dynamics and qEEG, Comput. Biol. Med. 152 (2023), 106418, https://doi.org/10.1016/j.compbiomed.2022.106418.

[7] N. Amoroso, D. Diacono, A. Fanizzi, M. La Rocca, A. Monaco, A. Lombardi, C. Guaragnella, R. Bellotti, S. Tangaro, Deep learning reveals Alzheimer's disease onset in MCI subjects: results from an international challenge, J. Neurosci. Methods 302 (2018) 3–9, https://doi.org/10.1016/j.jneumeth.2017.12.011.

[8] J. Sheng, B. Wang, Q. Zhang, R. Zhou, L. Wang, Y. Xin, Identifying and characterizing different stages toward Alzheimer's disease using ordered core features and machine learning, Heliyon 7 (2021), e07287, https://doi.org/10.1016/j.heliyon.2021.e07287.

[9] J. Zhang, L. Shi, Y. Shen, The retina: a window in which to view the pathogenesis of Alzheimer's disease, Ageing Res. Rev. 77 (2022), 101590, https://doi.org/10.1016/j.arr.2022.101590.

[10] H. Yu, X. Wu, L. Cai, B. Deng, J. Wang, Modulation of spectral power and functional connectivity in human brain by acupuncture stimulation, IEEE Trans. Neural Syst. Rehabil. Eng. 26 (2018) 977–986, https://doi.org/10.1109/TNSRE.2018.2828143.

[11] H. Yu, X. Li, X. Lei, J. Wang, Modulation effect of acupuncture on functional brain networks and classification of its manipulation with EEG signals, IEEE Trans. Neural Syst. Rehabil. Eng. 27 (2019) 1973–1984, https://doi.org/10.1109/TNSRE.2019.2939655.

[12] S. Bruzzone, M. Lumaca, E. Brattico, P. Vuust, M. Kringelbach, L. Bonetti, Dissociated brain functional connectivity of fast versus slow frequencies underlying individual differences in fluid intelligence: a DTI and MEG study, Sci. Rep. 12 (2022), 4746.

[13] L. Zhang, L. Wang, D. Zhu, Predicting brain structural network using functional connectivity, Med. Image Anal. 79 (2022), 102463, https://doi.org/10.1016/j.media.2022.102463.

[14] A. Alorf, M.U.G. Khan, Multi-label classification of Alzheimer's disease stages from resting-state fMRI-based correlation connectivity data and deep learning, Comput. Biol. Med. 151 (2022), 106240, https://doi.org/10.1016/j.compbiomed.2022.106240.

[15] H. Yu, X. Lei, Z. Song, C. Liu, J. Wang, Supervised network-based fuzzy learning of EEG signals for Alzheimer's disease identification, IEEE Trans. Fuzzy Syst. 28 (2020) 60–71, https://doi.org/10.1109/TFUZZ.2019.2903753.

[16] J. Sheng, B. Wang, Q. Zhang, Q. Liu, Y. Ma, W. Liu, M. Shao, B. Chen, A novel joint HCPMMP method for automatically classifying Alzheimer's and different stage MCI patients, Behav. Brain Res. 365 (2019) 210–221, https://doi.org/10.1016/j.bbr.2019.03.004.

[17] J. Sheng, B. Wang, Q. Zhang, M. Yu, Connectivity and variability of related cognitive subregions lead to different stages of progression toward Alzheimer's disease, Heliyon (2022), e08827.

[18] Z. Qing, F. Chen, J. Lu, P. Lv, W. Li, X. Liang, M. Wang, Z. Wang, X. Zhang, B. Zhang, Causal structural covariance network revealing atrophy progression in Alzheimer's disease continuum, Hum. Brain Mapp. 42 (2021) 3950–3962.

[19] M. Hejazi, A. Motie Nasrabadi, Prediction of epilepsy seizure from multi-channel electroencephalogram by effective connectivity analysis using Granger causality and directed transfer function methods, Cogn. Neurodyn. 13 (2019) 461–473, https://doi.org/10.1007/s11571-019-09534-z.

[20] R. Franciotti, N.W. Falasca, D. Arnaldi, F. Famà, C. Babiloni, M. Onofrj, F. M. Nobili, L. Bonanni, Cortical network topology in prodromal and mild dementia due to Alzheimer's disease: graph theory applied to resting state EEG, Brain Topogr. 32 (2019) 127–141.

[21] F. Azarmi, S.N. Miri Ashtiani, A. Shalbaf, H. Behnam, M.R. Daliri, Granger causality analysis in combination with directed network measures for classification of MS patients and healthy controls using task-related fMRI, Comput. Biol. Med. 115 (2019), 103495, https://doi.org/10.1016/j.compbiomed.2019.103495.

[22] B. Wang, Applying machine-learning methods based on causality analysis to determine air quality in China, Pol. J. Environ. Stud. 28 (2019) 3877–3885. 10.15244/pjoes/99639.

[23] C.W. Granger, Investigating causal relations by econometric models and cross-spectral methods, Econometrica (1969) 424–438.

[24] B. Wang, A novel causality-centrality-based method for the analysis of the impacts of air pollutants on PM2. 5 concentrations in China, Sci. Rep. 11 (2021) 1–9.

[25] A. Shojaie, E.B. Fox, Granger causality: a review and recent advances, Annu. Rev. Stat. Appl. 9 (2022) 289–319.

[26] C.L. Alves, A.M. Pineda, K. Roster, C. Thielemann, F.A. Rodrigues, EEG functional connectivity and deep learning for automatic diagnosis of brain disorders: Alzheimer's disease and schizophrenia, J. Phys. Complex. 3 (2022), 025001, https://doi.org/10.1088/2632-072X/ac5f8d.

[27] S. Hu, Y. Cao, J. Zhang, W. Kong, K. Yang, Y. Zhang, X. Li, More discussions for granger causality and new causality measures, Cogn. Neurodyn. 6 (2012) 33–42.

[28] S. Hu, G. Dai, G.A. Worrell, Q. Dai, H. Liang, Causality analysis of neural connectivity: critical examination of existing methods and advances of new methods, IEEE Trans. Neural Netw. 22 (2011) 829–844.

[29] G.-R. Wu, W. Liao, S. Stramaglia, J.-R. Ding, H. Chen, D. Marinazzo, A blind deconvolution approach to recover effective connectivity brain networks from resting state fMRI data, Med. Image Anal. 17 (2013) 365–374, https://doi.org/10.1016/j.media.2013.01.003.

[30] M. Ding, Y. Chen, S.L. Bressler, Granger causality: basic theory and application to neuroscience, in: Handbook of Time Series Analysis: Recent Theoretical Developments and Applications, 2006, pp. 437–460.

[31] A. Roebroeck, E. Formisano, R. Goebel, Mapping directed influence over the brain using Granger causality and fMRI, Neuroimage 25 (2005) 230–242, https://doi.org/10.1016/j.neuroimage.2004.11.017.

[32] M.F. Glasser, T.S. Coalson, E.C. Robinson, C.D. Hacker, J. Harwell, E. Yacoub, K. Ugurbil, J. Andersson, C.F. Beckmann, M. Jenkinson, A multi-modal parcellation of human cerebral cortex, Nature 536 (2016) 171–178.

[33] B. Wang, L. Li, L. Peng, Z. Jiang, K. Dai, Q. Xie, Y. Cao, D. Yu, A.D.N. Initiative, Multigroup recognition of dementia patients with dynamic brain connectivity under multimodal cortex parcellation, Biomed. Signal Process. Control 76 (2022), 103725.

[34] B. Fischl, FreeSurfer, Neuroimage 62 (2012) 774–781, https://doi.org/10.1016/j.neuroimage.2012.01.021.

[35] O. Esteban, C.J. Markiewicz, R.W. Blair, C.A. Moodie, A.I. Isik, A. Erramuzpe, J. D. Kent, M. Goncalves, E. DuPre, M. Snyder, H. Oya, S.S. Ghosh, J. Wright, J. Durnez, R.A. Poldrack, K.J. Gorgolewski, fMRIPrep: a robust preprocessing pipeline for functional MRI, Nat. Methods 16 (2019) 111–116, https://doi.org/10.1038/s41592-018-0235-4.

[36] E.W. Dickie, A. Anticevic, D.E. Smith, T.S. Coalson, M. Manogaran, N. Calarco, J. D. Viviano, M.F. Glasser, D.C. Van Essen, A.N. Voineskos, ciftify: a framework for surface-based analysis of legacy MR acquisitions, Neuroscience (2018), https://doi.org/10.1101/484428.

[37] M.F. Glasser, S.N. Sotiropoulos, J.A. Wilson, T.S. Coalson, B. Fischl, J.L. Andersson, J. Xu, S. Jbabdi, M. Webster, J.R. Polimeni, The minimal preprocessing pipelines for the Human Connectome Project, Neuroimage 80 (2013) 105–124.

[38] J.D. Ramsey, S.J. Hanson, C. Hanson, Y.O. Halchenko, R.A. Poldrack, C. Glymour, Six problems for causal inference from fMRI, Neuroimage 49 (2010) 1545–1558, https://doi.org/10.1016/j.neuroimage.2009.08.065.

[39] Q. Wang, C. He, Z. Wang, Z. Zhang, C. Xie, for the Alzheimer's Disease Neuroimaging Initiative, Dynamic connectivity alteration facilitates cognitive decline in Alzheimer's disease spectrum, Brain Connect. 11 (2021) 213–224, https://doi.org/10.1089/brain.2020.0823.

[40] S.M. Soman, S. Raghavan, P.G. Rajesh, N. Mohanan, B. Thomas, C. Kesavadas, R. N. Menon, Does resting state functional connectivity differ between mild cognitive impairment and early Alzheimer's dementia? J. Neurol. Sci. 418 (2020), 117093 https://doi.org/10.1016/j.jns.2020.117093.

[41] D. Putcha, M. Brickhouse, D.A. Wolk, B.C. Dickerson, Fractionating the Rey Auditory Verbal Learning Test: Distinct roles of large-scale cortical networks in prodromal Alzheimer's disease, Neuropsychologia 129 (2019) 83–92, https://doi.org/10.1016/j.neuropsychologia.2019.03.015.

[42] C.A. Leonards, B.J. Harrison, A.J. Jamieson, T. Steward, S. Lux, A. Philipsen, C.G. Davey, A distinct intra-individual suppression subnetwork in the brain's default mode network across cognitive tasks, Cerebral Cortex (2022) bhac361, doi: 10.1093/cercor/bhac361.

[43] J. Huber, M. Ruehl, V. Flanagin, P. zu Eulenburg, Delineating neural responses and functional connectivity changes during vestibular and nociceptive stimulation reveal the uniqueness of cortical vestibular processing, Brain Struct. Funct. 227 (2022) 779–791, https://doi.org/10.1007/s00429-021-02394-6.

[44] J. Qiao, Y. Lv, C. Cao, Z. Wang, A. Li, Multivariate deep learning classification of Alzheimer's disease based on hierarchical partner matching independent component analysis, Front. Aging Neurosci. 10 (2018) 417, https://doi.org/10.3389/fnagi.2018.00417.

[45] A. Khazaee, A. Ebrahimzadeh, A. Babajani-Feremi, Classification of patients with MCI and AD from healthy controls using directed graph measures of resting-state fMRI, Behav. Brain Res. 322 (2017) 339–350, https://doi.org/10.1016/j.bbr.2016.06.043.

[46] S.L. Warren, A.A. Moustafa, Functional magnetic resonance imaging, deep learning, and Alzheimer's disease: a systematic review, J. Neuroimaging 33 (2023) 5–18, https://doi.org/10.1111/jon.13063.